MODELING AND SIMULATION BASED ON FINITE ELEMENT METHOD FOR ELECTRON BEAM WELDING PROCESS

Zhengkun Feng[(a)], Henri Champliaud[(b)]

Department of Mechanical Engineering,
Ecole de technologie superieure
1100 Notre-Dame Street West,
Montreal, Quebec, H3C 1K3, Canada

[(a)]zhengkun.fengca@etsmtl.ca, [(b)]henri.champliaud@etstmtl.ca

ABSTRACT
Electron beam welding is a type of welding with high energy density that provides advantage for welding thick parts of high strength metal with single pass. In this paper, the development of a thermal structural model based on finite element method is presented. A conical heat source model is applied in the model. The temperature distribution and time history are reported with numerical simulation results. The residual stresses in the fusion zone and the heat affected zones have been analyzed.

Keywords: electron beam welding, conical heat source, Finite element analysis, Residual stress, ANSYS

1. INTRODUCTION

Since the environment protection gets increasing attention, high strength metals have more applications in industries. Electron beam welding has many advantages over other welding. This welding process provides deep penetration and does not require prepared welding groove and filler material and single pass can be performed for welding thick parts of high strength metals. Moreover, small heat affected zones can be obtained by this welding. During electron beam welding, the electron beam strikes the surface of the metal. As a result, melts evaporates and a hole is created. As the surface of the hole is continuously struck by the electron beam and the surface of the hole evaporates continuously, a keyhole is drilled by the electron beam metal (Andrews and Atthey 1976; Ho et al. 2007).

With the fast evolution of computing technology, modeling and simulation of complex process and system with large dimension becomes possible. Three-dimensional modeling of electron beam welding can be found in the late 1980's (Lindgren and Karlsson 1988). Rai et al. (2009) and Adamus et al. (2013) performed analyses of electron beam welding on thin plates. Lacki and Adamus (2011) performed numerical simulations of electron beam welding for joining tubes with different thicknesses. In this paper, a thermal-structural model based on finite element method is presented. The geometry of the specimen to be welded is illustrated in Fig. 1. A conical heat source model is applied to the thermal-structural model. The temperature and stress distributions obtained from the numerical simulation results will be reported and discussed.

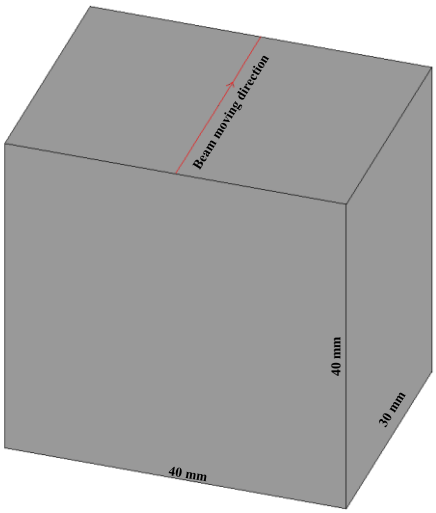

Figure 1: Geometrical set up

2. PROCESS MODELING BASED ON FINITE ELEMENT METHOD

As the geometry of the specimen was symmetric to the electron beam moving direction, when building the model, the boundary conditions were selected to make the deformation to be symmetric. Therefore, for the sake of saving CPU time when performing numerical simulations, only one half of the specimen was required for the symmetric model (Fig. 2). In the figure, yz plane was the symmetric plane and y was the electron beam moving direction. The numerical model based on finite element method with implicit time integration scheme was built on ANSYS platform. The model was divided into two parts: the thermal and structural parts. 8-node thermal and structural cubic elements were respectively selected for the mesh of the model with 38400 elements in the fine zone with 8 mm of width and 19200

elements in the coarse zone with 32 mm of width. The degrees of freedom (nodal temperature in the thermal part, nodal displacement u_x, u_y and u_z in the structural part) between the nodes of the fine and the coarse zones were coupled. Since the deformation was assumed to be small, thermal structural uncoupled sequential model was selected. The thermal part provided the temperature distributions at each instant during the welding as information to be used by the structural part to calculate the thermal expansion during the welding. For preventing the specimen from rigid body movement, u_y and u_z were zero at points (0, 0, -0.04), and u_z was zero at points (0, 0.03,-0.04). The material had the density of 7860 kg/m^3 and Poisson ratio of 0.3. The other thermal and mechanical properties, such as the enthalpy H, the conductivity coefficient k, the convective coefficient h_f, the thermal expansion coefficient α, the Young's modulus E and the yield stress S_y were dependent of temperature as shown in table 1. The elastic-perfect-plastic bilinear material model with the Young's modulus E and the yield stress S_y was applied. The following conical heat flux distribution (Luo et al. 2010) was selected:

$$q = q_0 e^{\frac{-3h^2}{(z+h)^2}\left(\frac{x^2+y^2}{r_0^2}\right)} \quad (1)$$

where q denotes the heat flux in the conical zone; q_0 denotes the heat flux at the center of the cone; h denotes the depth of the heat source; r_0 denotes the radius of the cone bottom. In the model, q_0, h, r_0 were selected as 137 W/mm^3, 60 mm, 2 mm.

Table 1: Thermal and mechanical properties of material

T (^{o}C)	H (MJ/m^3)	k (W/^{o}Cm)	h_f (W/^{o}Cm^2)	α (10^{-6}/^{o}C)	E (GPa)	S_y (MPa)
20	0	51	9.5	12.18	165	345
100	296	49.5	11.8	12.18	180	
200	685	48	16.3	12.66	195	280
400	1544	42	30.8	13.47	173	150
600	2603	37	54.8	14.41	88	55
800	4840	26	90.8	12.64	75	40
1000	5859	26	141	13.37	70	15
1200	6877	28	208.1		60	
1400	7936	28	294.4		30	
1490	8412	50	340.8		17	
1570	10512	80	384.8		10	
1700	11200	120	465.4		10	
5000	28668	125	500		10	

3. SIMULATION RESULTS AND DISCUSSIONS

In the welding simulation, the simulation time was 5 seconds with the speed of the electron beam of 6 mm/s. Firstly, the thermal simulation was carried out with the thermal part of the model. Then, the structural simulation was carried out with the structural part of the model as described in section 2.

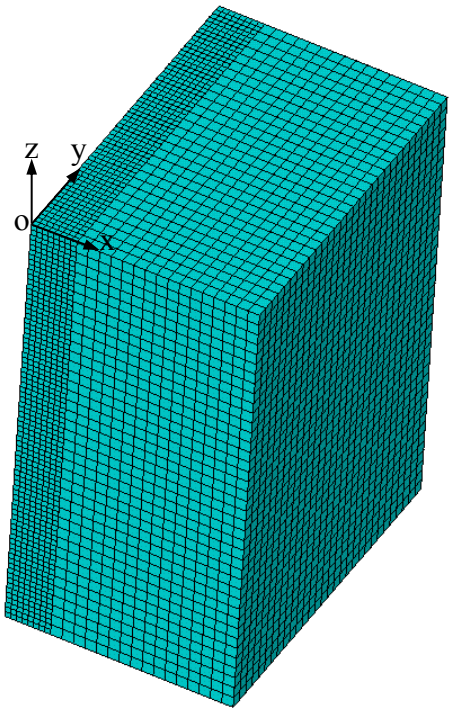

Figure 2: non-uniform mesh of the model with 8-node solid elements

3.1. Thermal Simulations

The initial temperature of the specimen was 20 ^{o}C. It was assume that the welding was performed in vacuum chamber. The convective coefficients were selected as 100 time less than those listed in table 1. Figure 3 shows the temperature distribution on the cutting plane perpendicular to the beam moving direction at the instant of 3 second (For the clarity, the results are presented in complete model instead of symmetric model). It was observed that the temperature distribution was in conical shape. Figure 4 shows the temperature distribution on the symmetric plane at the instant of 3 second. After the welding, the specimen was cooled at free convection on all surfaces by air at room temperature of 20 ^{o}C. The convective coefficients were selected as shown in Table 2. As the temperature gradient of the specimen at the beginning was high, a small constant time step at the first 2 seconds was used to ensure the convergence. However, the temperature gradient became smaller and continued to rapidly decrease after 2 seconds. For the sake of CPU time, the current time step proportionally greater than each previous time step was selected. The total cooling time was 6 hours and the specimen temperature became 20 ^{o}C. Figure 5 shows the temperature distribution on the symmetric plane at the instant of 61 second that corresponding of the instant of 56 second after the start of the cooling. As the electron beam welding is a type of welding with high energy density and the heat affect zone is small, the temperate gradients in the center of the conical heat source and nearby are very strong. The

temperature gradient of point C near the instant of 2.5 second was the highest when the electron beam center reached to this point. This point was the geometric center of the specimen (Fig. 7). Figure 8 shows the temperature distributions on the cross line AB (Fig. 7) that passed through the specimen center and was perpendicular to the electron beam moving direction at different instants. It was observed that the temperature gradient at the position x of zero between instants 3 second and 6 second was much stronger than that between instants 6 second and 61 second. The nearby positions had the same temperature distribution tendencies.

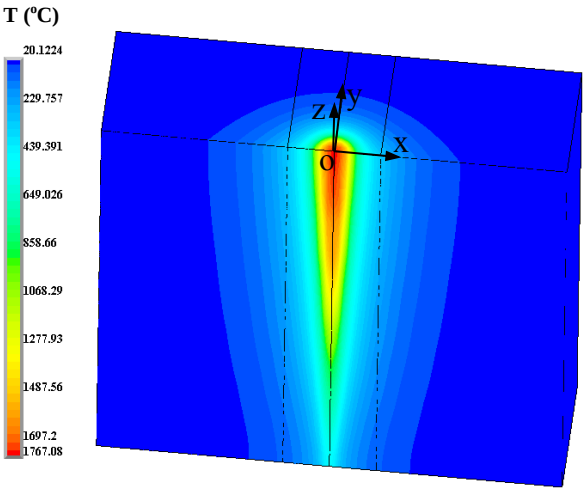

Figure 3: Temperature distribution on the cutting plane perpendicular to the beam moving direction at 3 second

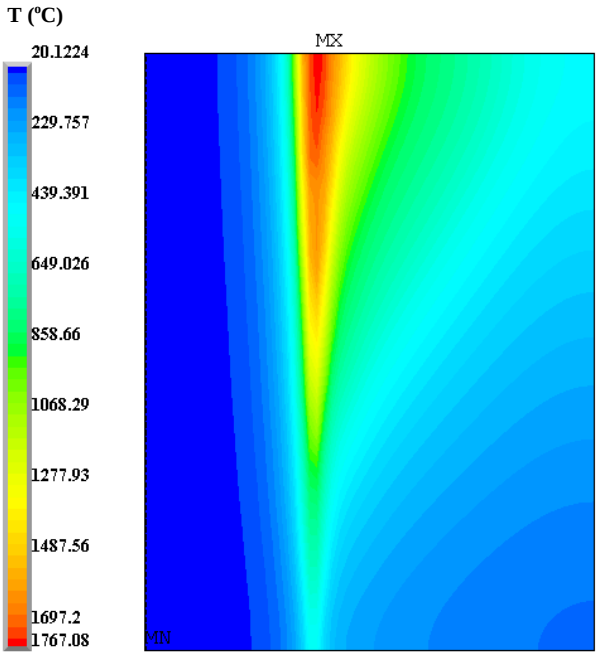

Figure 4: Temperature distribution on the symmetric plane at 3 second

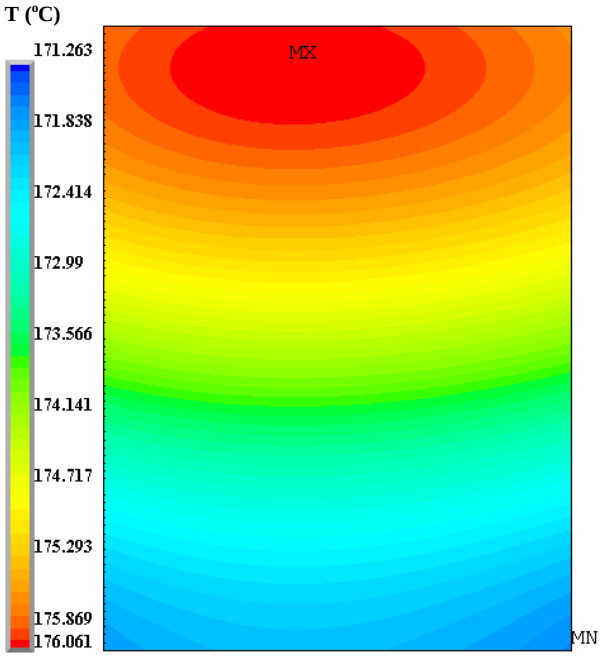

Figure 5: Temperature distribution on the symmetric plane at 61 second

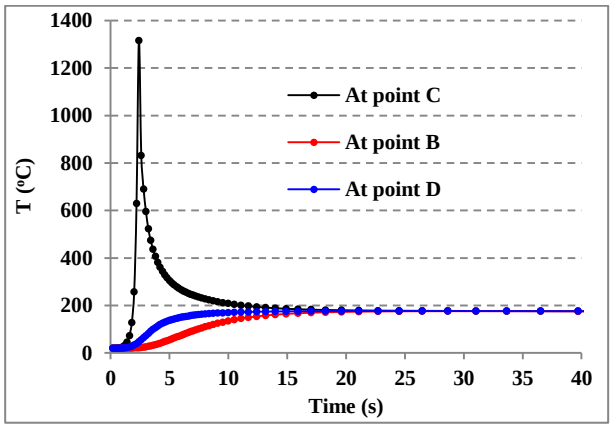

Figure 6: Temperature histories at seclected positons

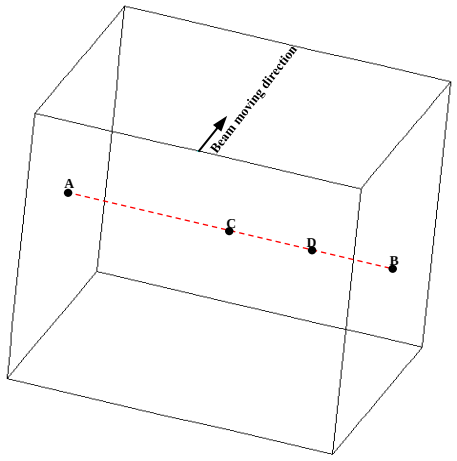

Figure 7: Position of the seclected points and the cross line

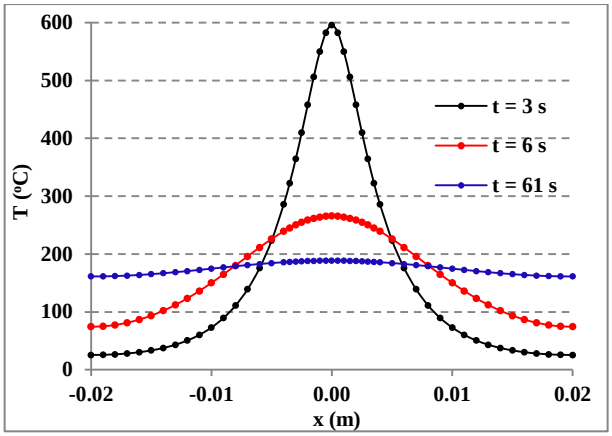

Figure 8: Temperature istributions on the cross line at different instants

3.2. Structural Simulations

After performing the thermal simulation, the temperature at each node of the model of the specimen was saved. According to this information with thermal properties, such as the thermal expansion coefficients and the mechanical properties of the specimen at different temperature, a structural simulation was performed with the structural part of the model to assess the electron beam welding process. Figure 9 shows the Von Mises stress histories of the three points in Fig. 7. It was observed that the Von Mises stress variations during the welding was very strong and got the values that approached to the final values. The Von Mises stress located at the center point C was higher than that at the point B located at the side surface and the one at the point D located between these two points. Figure 10 shows the residual stress distributions on the cross line AB of Fig. 7. The Von Mises residual stress was not at the center of the specimen but at a point in the heat affected zone with a distrance of 6 mm from the center of the speciment. In addition, it was observed that there were a zone where the stress in the plane perpendicular to the thickness direction was compressive. Figure 11 shows the Von Mises stress distribution on the cross section cutting through line AB of Fig. 7 and perpendicular to the electron beam moving direction. It was observed that the maximum value was located at a point between points C and D. Figure 12 shows the Von Mises stress distributions on the cross sections perpendicular to the electron beam moving direction and cutting from the welding starting point A with distances of 2.5 mm, 7.5 mm, 12.5 mm, 17.5 mm, 22.5 mm and 27.5 mm, respectively. It was observed the Von Mises stress distribution partner was established in the range from 2.5 mm to 2.75 mm in the electron beam moving direction.

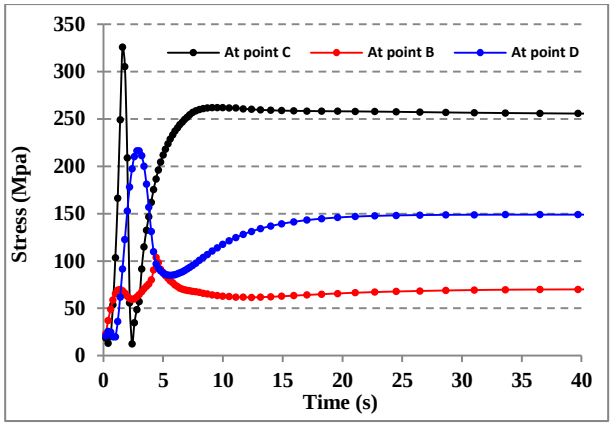

Figure 9: Von Mises stress histories at seclected positons

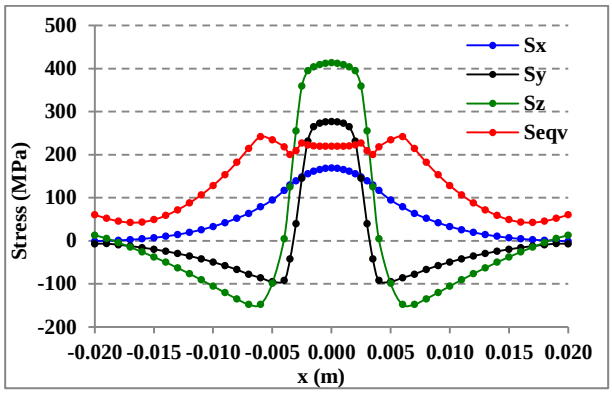

Figure10: Residual stress distributions on the cross line AB

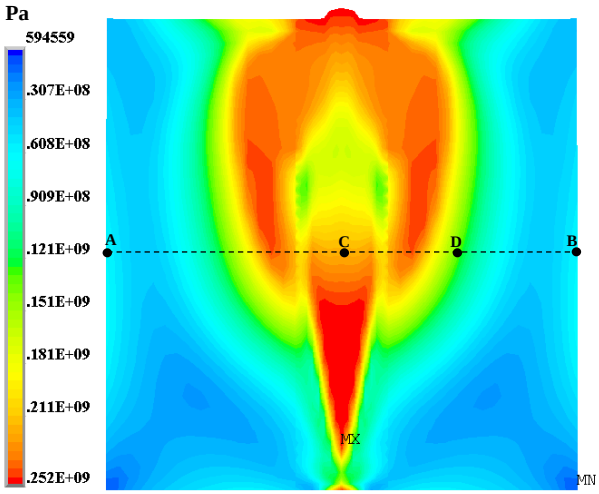

Figure 11: Residual Von Mises stress distribution on the cross section at the mid length

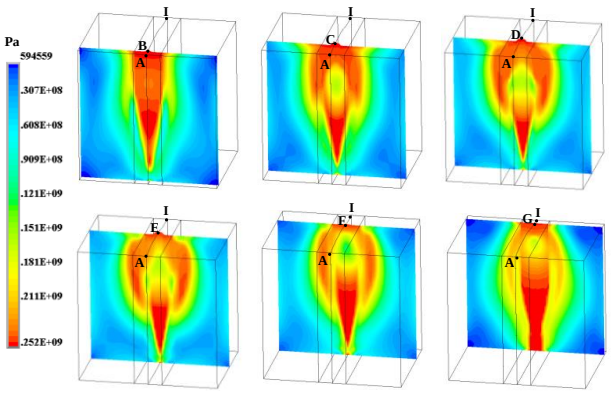

Figure12: Residual Von Mises stress distributions on different cross sections

4. CONCLUSIONS

The numerical model for electron beam welding process shows that this type of welding with high energy density provides deep penetration and is capable of welding thick parts of high strength metals. It shows also that the welding can be performed without prepared welding groove and with single pass. The heat affected zones are relatively small. However, reducing the maximum residual stress and the heat affected zones by pre-heating and/or post heating and validating the model with experimental results remain for the ongoing work.

ACKNOWLEDGMENTS

The authors thank the Natural Sciences and Engineering Research Council (NSERC), Alstom Hydro Canada Inc. and Hydro Quebec for their financial supports to this research.

REFERENCES

Adamus, K., Kucharczyk, Z., Wojsyk, K., and Kudla, K. (2013). Numerical analysis of electron beam welding of different grade titanium sheets. *Computational Materials Science*, 77, 286-294. doi: 10.1016/j.commatsci.2013.05.001

Andrews, J. G., and Atthey, D. R. (1976). Hydrodynamic limit to penetration of a material by a high-power beam. *Journal of Physics D: Applied Physics*, 9(15), 2181-2194. doi: 10.1088/0022-3727/9/15/009

Ho, C. Y., Wen, M. Y., and Lee, Y. C. (2007). Analytical solution for three-dimensional model predicting temperature in the welding cavity of electron beam. *Vacuum*, 82(3), 316-320. doi: 10.1016/j.vacuum.2007.04.040

Lacki, P., and Adamus, K. (2011). Numerical simulation of the electron beam welding process. *Computers and Structures*, 89(11-12), 977-985. doi: 10.1016/j.compstruc.2011.01.016

Lindgren, L.-E., and Karlsson, L. (1988). Deformations and stresses in welding of shell structures. *International Journal for Numerical Methods in Engineering*, 25(2), 635-655.

Luo, Y., Liu, J., Ye, H., and Shen, B. (2010). Numerical simulation on electron beam deep penetration welding and weld appearance of magnesium alloy. *Hanjie Xuebao/Transactions of the China Welding Institution*, 31(6), 65-68.

Rai, R., Burgardt, P., Milewski, J. O., Lienert, T. J., and Debroy, T. (2009). Heat transfer and fluid flow during electron beam welding of 21Cr-6Ni-9Mn steel and Ti-6Al-4V alloy. *Journal of Physics D: Applied Physics*, 42(2). doi: 10.1088/0022-3727/42/2/025503